

Remote Excitation of Tip-Enhanced Photoluminescence with a Parallel AgNW Coupler

Wannes Peeters, Shuichi Toyouchi,* Yasuhiko Fujita,* Mathias Wolf, Beatrice Fortuni, Eduard Fron, Tomoko Inose, Johan Hofkens, Takahiko Endo, Yasumitsu Miyata, and Hiroshi Uji-i*



Cite This: *ACS Omega* 2023, 8, 38386–38393



Read Online

ACCESS |



Metrics & More

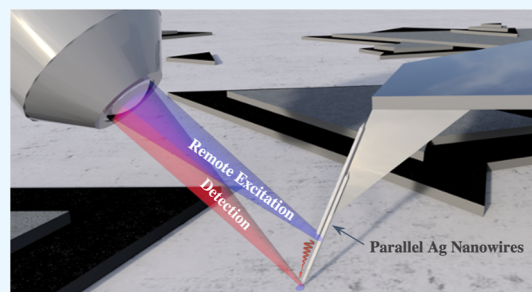


Article Recommendations



Supporting Information

ABSTRACT: Tip-enhanced photoluminescence (TEPL) microscopy allows for the correlation of scanning probe microscopic images and photoluminescent spectra at the nanoscale level in a similar way to tip-enhanced Raman scattering (TERS) microscopy. However, due to the higher cross-section of fluorescence compared to Raman scattering, the diffraction-limited background signal generated by far-field excitation is a limiting factor in the achievable spatial resolution of TEPL. Here, we demonstrate a way to overcome this drawback by using remote excitation TEPL (RE-TEPL). With this approach, the excitation and detection positions are spatially separated, minimizing the far-field contribution. Two probe designs are evaluated, both experimentally and *via* simulations. The first system consists of gold nanoparticles (AuNPs) through photoinduced deposition on a silver nanowire (AgNW), and the second system consists of two offset parallel AgNWs. This latter coupler system shows a higher coupling efficiency and is used to successfully demonstrate RE-TEPL spectral mapping on a MoSe₂/WSe₂ lateral heterostructure to reveal spatial heterogeneity at the heterojunction.



INTRODUCTION

In recent years, there has been an ever-increasing demand for methods able to provide spectroscopic data on the nanoscale due to, *e.g.*, the advancing miniaturization of electronic and optoelectronic devices,^{1–4} DNA mapping,^{5–8} fundamental research into biological pathways,^{9,10} *etc.* Conventional light microscopes are typically limited by the diffraction limit and can, thus, only provide information on the scale of a few hundred nanometers.¹¹ In order to satisfy the demand for higher spatial resolutions, a variety of methods are available that are commonly grouped as super-resolution microscopy techniques. A few examples of the developed techniques are stimulated emission depletion microscopy (STED)^{12–14} which makes use of a secondary, usually donut-shaped, high-power laser beam to deplete the fluorescent signal everywhere except at the center of the donut, and single molecule localization based microscopies such as photoactivated localization microscopy (PALM, S-PALM)^{15,16} and stochastic reconstruction microscopy (STORM, d-STORM, NASCA, ...)^{17–20} which make use of the stochastic nature of fluorophore properties at the single molecule level to switch on subsets of labels to achieve single molecules localization followed by image reconstruction and tip-enhanced spectroscopy (TES), which uses a tip to locally enhance the spectroscopic processes to generate higher resolution images.²¹ TES provides Raman^{22–25} and/or photoluminescence (PL)^{26,27} data along with all the information provided by scanning probe microscopy (SPM), such as topography, tip–sample inter-

actions, sample composition, work function, electrical properties, mechanical properties *etc.*, with nanometer resolution.^{27,28} TES is achieved by locally enhanced electromagnetic (EM) fields with nanosized plasmonically active probes.²⁹ This local enhancement is mainly attributed to two effects, the lightning rod effect³⁰ and localized surface plasmon resonance (LSPRs).³¹ To concentrate the excitation volume even further, a plasmonic substrate can be used, which can lead to substantially higher enhancements (known as gap mode).^{32,33} In a nanogap between a plasmonic probe and substrate, enhancements as high as 6×10^5 have been reported for dark excitons.³⁴ However, especially for tip-enhanced photoluminescence (TEPL), there is a drawback in the gap-mode configuration, as the plasmonic substrate can significantly introduce nonradiative energy transfer through Ohmic losses in metals, resulting in PL quenching.³⁵ Moreover, in the fields of electronics/optoelectronics and biology, insulating non-plasmonic substrates, such as mica, glass, and silicon wafers, are preferred. Thus, the gap-mode enhancement cannot be utilized in most cases, making this approach not broadly applicable. Furthermore, to achieve high-resolution images, the PL

Received: July 11, 2023

Accepted: September 5, 2023

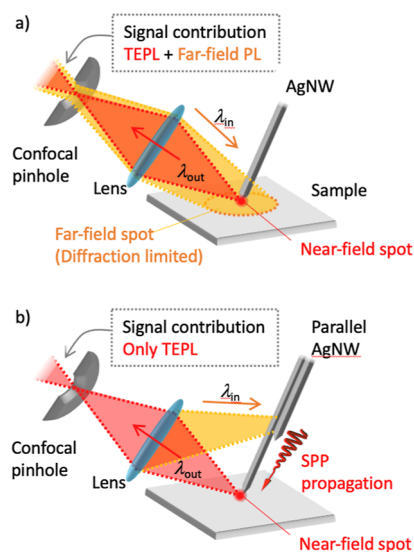
Published: September 20, 2023



enhancement must be sufficiently high to overcome the background signal generated by the far field. Although a high spatial resolution of 5 nm has been reported on nonplasmonic substrates,²⁶ and even subnanometer resolutions have been achieved using gap-mode methodology,³⁶ such high resolutions can only be realized with specific samples (*e.g.*, a low density of quantum dots) and/or experimental conditions (*e.g.*, cryogenic ultrahigh vacuum). This indicates that the applicability of TEPL is still limited, and methodologies for improving TEPL contrast by either signal enhancement or far-field background suppression are in high demand.

In light of this, we have developed a versatile method that eliminates the far-field signal from the detection pathway through the concept of remote excitation (RE).^{25,37,38} In traditional TES, the excitation spot and detection spot are spatially overlapped, as illustrated in Scheme 1a (known as

Scheme 1. Schematic Representation of the Direct and RE Principles; in Direct Excitation (a), the Incident Laser Light and the Detection Points Are Both Aligned to the AgNW Apex, Meaning That Detection Contains Both the Far-Field Background and Near-Field Contribution; in Contrast, in RE (b), the Laser Light Is Misaligned, Away from the Detection Point, and Focused onto a Light Coupling Point, Allowing for SPP Propagation and LSPRs at the Apex⁴



⁴This misaligned configuration enables efficient detection of the near-field signals by blocking the background signals with the pinhole.

direct excitation). Differently, in the RE configuration, the laser excitation and the detection spots are physically separated (Scheme 1b). This type of excitation is made possible by coupling light into surface plasmon polaritons (SPPs) on a silver nanowire (AgNW).^{39,40} These SPPs are then able to propagate over the AgNW and localize at the apex to generate highly enhanced near-field EM (LSPRs). This allows for any signals that are directly excited by the incident laser light and its scattering to be blocked by the confocal pinhole. In such a way, the near-field signal from the sample of interest can be effectively decoupled from the far-field background, which leads to a vast increase in contrast. Chemically synthesized AgNWs are especially promising materials for this purpose due to their high crystallinity and atomically smooth surface, resulting in low radiation damping and low Ohmic losses at

both visible and near-infrared light frequencies.⁴¹ While a key aspect of this technique is the ability of the far-field excitation light to couple into SPPs, this is not trivial due to the momentum mismatch between SPPs and far-field light.⁴² Although light coupling is possible at the apex of AgNW since the sharp features allow for momentum matching, this is not the case at the middle section of a AgNW.^{43,44} Several solutions have been reported to facilitate the coupling of light into SPPs, ranging from attaching plasmonic nanoparticles through alternating current electrophoresis,²⁵ or physical deposition by using a micromanipulator,⁴⁰ and even fabricating a coupler through ion beam milling.^{22,45,46} Despite this, a short SPP decay length (*e.g.*, 1.3 μm @ 532 nm for AgNWs)⁴⁷ as well as the low coupling efficiency obstruct current TES contrast/applicability.

Our experimental and simulation findings validate the higher coupling efficiency of the proposed novel probe design over the conventional AgNW probe design, which uses plasmonic NPs deposited on a nanowire as the coupling point. The potential of the parallel AgNW (pNW) probe is supported by comparing their performance in standard confocal microscopy, direct excitation TEPL, and RE-TEPL microscopy on a lateral heterostructure of monolayer $\text{MoSe}_2/\text{WSe}_2$. We found that the pNW coupler system not only effectively suppresses the appearance of far-field optical artifacts, typical of TEPL measurements, but also allows us to reveal previously unattainable spatial heterogeneity of the electronic structures of the 2D materials thanks to the decoupling of the far-field contribution by the RE. These findings mark a significant leap forward in the field of TES, as the design of the pNW probe outperforms traditional methods by a substantial margin. Our novel approach opens up exciting possibilities for nanoscale spectroscopic imaging, with potential applications across a wide range of scientific and industrial disciplines. By eliminating limitations in conventional probe designs, it offers a new tool to gain valuable insights into nanoscale phenomena.

RESULTS AND DISCUSSION

The SPP properties of the light-coupling systems are compared (Figure 1a). For both systems, the AgNWs used as plasmonic waveguides were synthesized *via* a water-mediated polyol process previously reported by our group (Supporting Information-1), which enables obtaining pencil-like sharp AgNWs.⁴⁸ The synthesized AgNWs possess sharp ends with an apex radius of ~ 25 nm, suitable for SPM applications. For the NPs coupler system, Au NPs were deposited using site-specific photoreduction of gold ions on a AgNW (Supporting Information-1).⁴⁷ The pNW coupler was fabricated by aligning two AgNWs with physical manipulation (Figures S1 and S2). The deposited AuNPs and the junction of two AgNW offsets were employed as the light-coupling points, respectively (Figure 1a). The SPP properties are investigated both numerically and experimentally. Figure 1b represents FDTD simulations of the couplers. The detailed information about the simulation is described in Supporting Information-3. For this simulation, the light-coupling point was located 2.5 μm from the AgNW end. In both coupling systems, incident light polarized perpendicular to the longitudinal axis of the AgNWs demonstrated the best coupling efficiency. Comparing the electric field intensity ($|E|^2$) at the distal end of the AgNW, the LSPRs at the tip apex with the pNW coupler were estimated to be 10^3 times higher than those with the NP coupler (Figure 1b). This was likely because of (i) the higher coupling

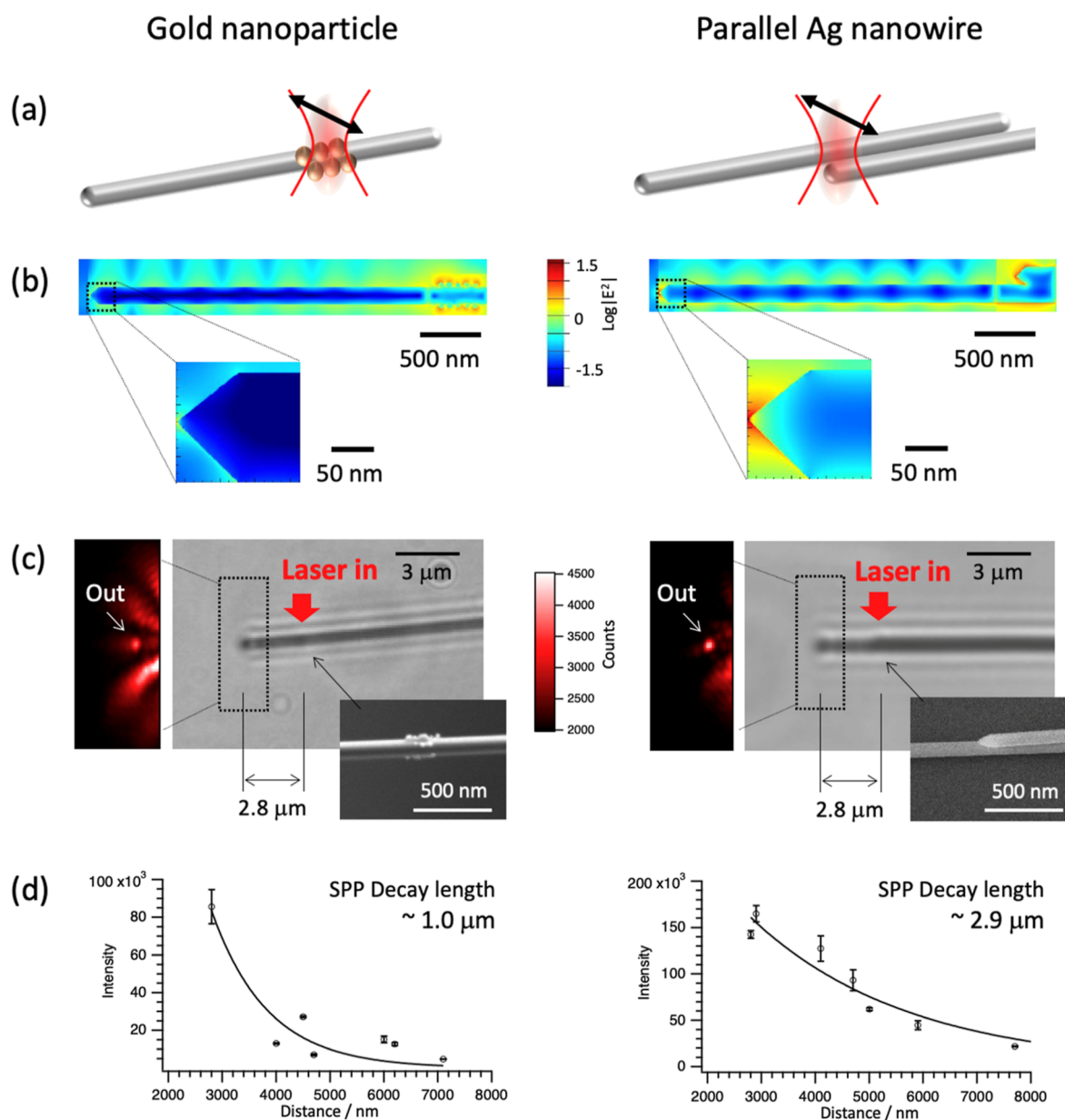


Figure 1. Comparison proposed light-coupling geometries: *in situ*-fabricated AuNPs (left) and a pair of parallel AgNW (right), respectively. (a) Schematic illustration of light-coupling geometries. In both cases, light polarization was set to be perpendicular to the longitudinal axis of the AgNW. (b) Numerically simulated electronic field intensity along the AgNW. (c) CCD image showcasing both geometries with a coupling point at 2.8 μm (AuNP coupler at left and pNW coupler at right, respectively); the inset to the left shows the CCD image of out-coupling light from the distal end of the AgNW, and the inset on the bottom shows a SEM image of the coupling point, respectively. (d) Integrated intensity of out-coupling light at the distal end as a function of the coupling point distance from the end. The laser power used in (c,d) was 25 W/cm².

efficiency at the pNW coupler compared to the NP coupling system, (ii) the lower Ohmic losses of Ag compared to Au,⁴⁹ and (iii) the better resonance property on the pNW system (Figure S3).

Experimentally, the SPP was excited by focusing laser light of 632.8 nm at the coupling points, and the out-coupling far-field light from the distal end of the AgNWs was detected with a CCD camera (see the experimental conditions in Supporting Information 4). Figure 1c shows typical experimental results where the coupling points were located 2.8 μm away from the nanowire end. Although out-coupling light was clearly detected in both systems, the intensity in the pNW coupler system was significantly higher than that in the NP coupler system (the left inset of Figure 1c). In addition, a much lower scattering light

from the coupling point was detected in the case of the pNW coupler system.

The out-coupling light intensity exponentially depends on the distance of the coupling point from the distal end (Figure 1d). From the decay curves, the SPP decay length in the pNW system was estimated to be $\sim 2.9 \mu\text{m}$, which was 3 times longer than that in the NP system ($\sim 1.0 \mu\text{m}$). The SPP decay length was defined as the distance at which the SPP intensity reached $1/e$ of the initial intensity by fitting the intensity of the experimental and simulated data. The longer SPP decay length, as well as intense out-coupling with the pNW system, were consistent with the FDTD simulations. This set of simulations and experiments suggests that the pNW coupler system would be well-suited for RE-TEPL microscopy.

For RE-TEPL microscopy, the coupler system was attached to an SPM probe. This was achieved by first fabricating the parallel AgNWs on an ITO substrate, followed by transferring the two AgNWs to an AFM cantilever (the detailed protocol is in Supporting Information-5 and Figure S5). An example of the SEM image of the fabricated parallel AgNW probe is shown in Figure 2. The distance from the coupling point to the

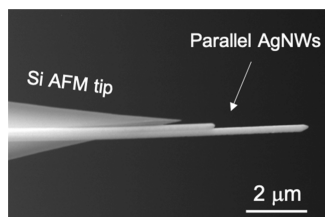


Figure 2. SEM image of parallel AgNWs attached to a commercial silicon AFM cantilever (pNW probe).

nanowire apex was optimized to be about $3.5 \mu\text{m}$ in order to block scattering light at the coupling point with the confocal pinhole in our TEPL setup (Figure S6).

To validate the TEPL activity of the probes, transition-metal dichalcogenides (TMD) monolayers, consisting of a lateral heterostructure of monolayer $\text{MoSe}_2/\text{WSe}_2$,^{50,51} deposited on Si/SiO₂ were used as a standard sample. The TMD monolayer consists of a MoSe_2 inner region surrounded by a WSe_2 outer region within a single atomic layer. The MoSe_2 inner region efficiently emits luminescence centered at $\sim 1.52 \text{ eV}$ ($\sim 815 \text{ nm}$), while the luminescence of the WSe_2 is centered around 1.58 eV ($\sim 785 \text{ nm}$) with a relatively low yield (Figure S7). At

the junction between MoSe_2 and WSe_2 , the energy states of these TMDs are considered to be slightly modified due to the possible crystal strain and/or their complicated intrinsic exciton migration dynamics, which occur at the nanoscale (well below the diffraction limit). Figure 3a,b displays an optical reflection image and a diffraction-limited confocal luminescence image, excited at 632.8 nm , of a $\text{MoSe}_2/\text{WSe}_2$ heterostructure. An AFM topographic image of the junction is shown in Figure 3c. This AFM image was taken with the pNW probe. Because the tip radius of the sharp AgNWs used in this study was $\sim 25 \text{ nm}$, the AFM images recorded with an AgNW probe have a resolution of $\sim 25 \text{ nm}$. Thanks to this, the detailed structure of the TMD monolayer at the nanoscale, such as contaminations, the edge of monolayers, and the heterojunction between MoSe_2 and WSe_2 , could be clearly visualized (Figures 3c and S7). During TEPL measurements, the probe was positioned on the MoSe_2 part, and consecutive measurements were performed with the probe in contact (tip-in) or the probe removed out of the image plane (tip-out), corresponding to tip-enhanced and conventional far-field spectroscopy, respectively. The signal that was recorded with the tip-out configuration represents the background signal created by the far-field contribution. In the case of direct excitation (Figure 3d), luminescence peaking around 815 nm was detected in both tip-in and tip-out configurations. The contribution of the far-field was substantial, and TEPL contrast, defined as $I_{\text{tip-in}}/I_{\text{tip-out}}$, was estimated to be ~ 1.6 . Upon switching to RE, as illustrated in Figure 3e, due to a significant reduction in far-field contribution, the TEPL contrast was estimated to be ~ 12.0 , which is more than 7 times higher than that obtained with direct excitation. (The

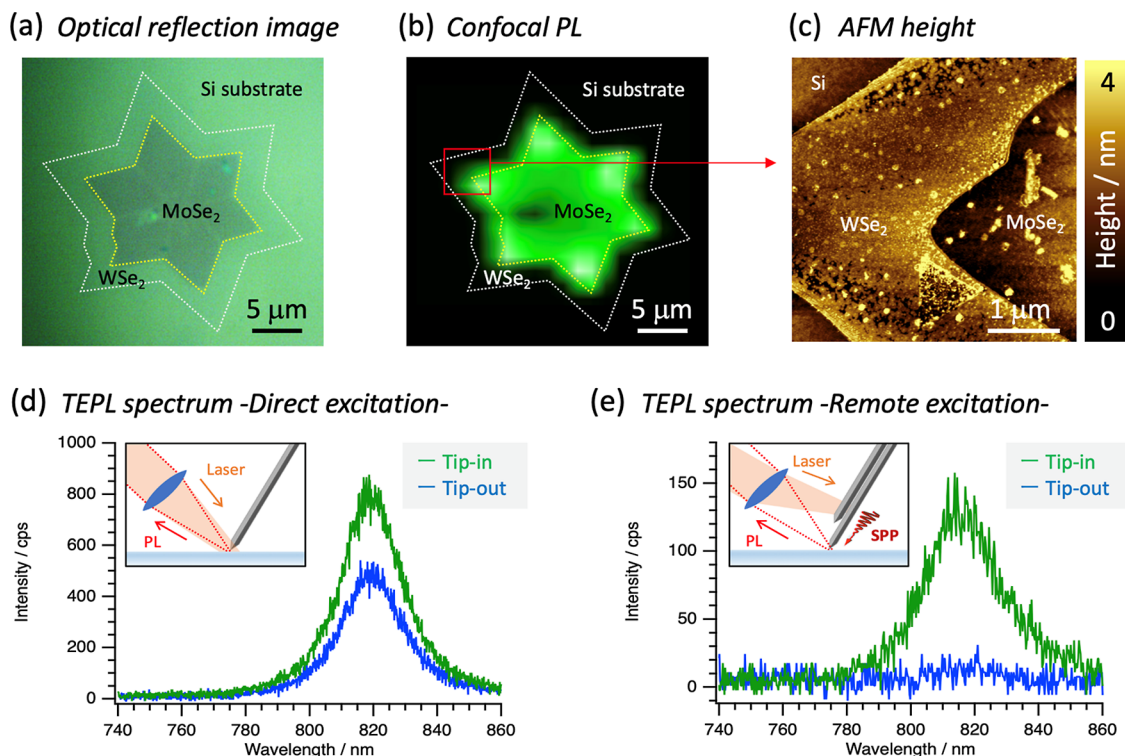


Figure 3. Comparison between the direct and RE of TEF. (a) Optical reflection image of a monolayer of $\text{MoSe}_2/\text{WSe}_2$ lateral heterostructure on a Si/SiO₂ substrate. (b) Confocal photoluminescence image of the $\text{MoSe}_2/\text{WSe}_2$ monolayer (60 \times objective NA 0.95, excited at 632.8 nm). (c) AFM image of the area indicated in (b) with the red square showcasing the monolayer heterostructure taken with the pNW probe. TEPL spectra (green lines) and luminescence spectra taken without the pNW probe (blue line) were recorded *via* direct excitation (d) and RE (e).

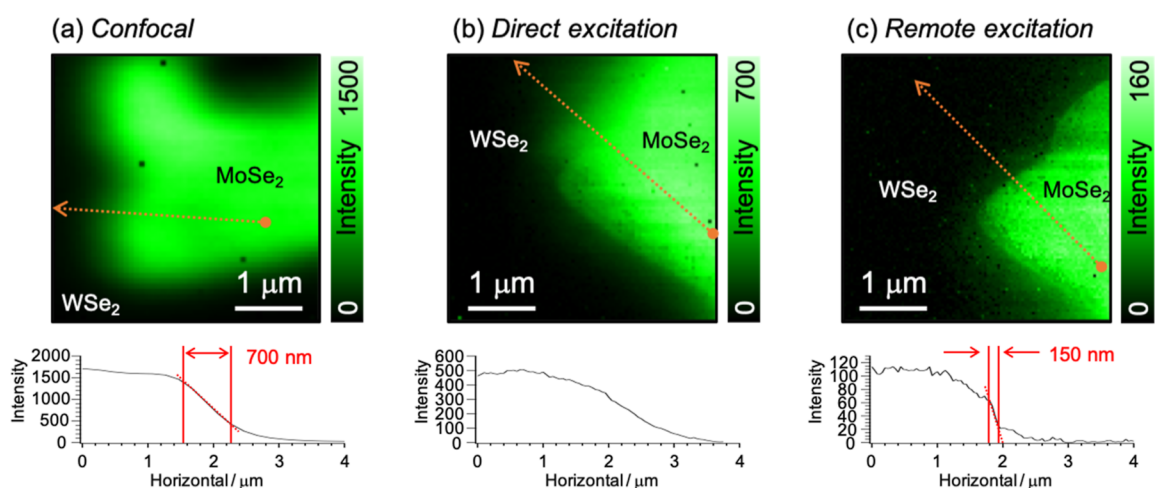


Figure 4. Comparison between diffraction-limited confocal microscopy direct excitation TEPL and RE TEPL images of heterostructure MoSe₂/WSe₂ on a Si/SiO₂ substrate. Photoluminescence intensity mapping of MoSe₂ for (a) confocal, (b) direct excitation TEPL, and (c) RE-TEPL in which the dashed arrows indicate the line profiles plotted of respectively the confocal mapping, the TEPL mapping, and the RE-TEPL mapping. The confocal map was collected with a 60× NA0.95 objective, and the TEPL and RE-TEPL maps were recorded with a 100× NA0.7 objective.

detailed experimental configuration of TEPL is displayed in Figure S8.)

To corroborate these findings, a comparison of PL mapping was made between confocal microscopy, direct excitation TEPL, and RE-TEPL microscopy on the heterostructure (Figure 4). Direct excitation and RE-TEPL measurements were conducted with the same pNW probe at the same location of the sample. The maps shown in Figure 4 all focus on the MoSe₂/WSe₂ heterojunction, and the maps were constructed using luminescence from MoSe₂. When looking at the TEPL map under direct excitation (Figure 4b), a slight improvement in image contrast was already observed compared to the confocal image (Figure 4a). The direct excitation TEPL map was, however, likely convoluted with an additional far-field shadow, as seen in the upper part of the map in Figure 4b. Due to the presence of these far-field contributions, improvement of the spatial resolution against the confocal is not clearly seen from the line profile shown in Figure 4b bottom. In contrast, the RE-TEPL map exhibited an evident improvement, likely owing to the suppression of the far-field contributions. The corresponding line profile confirmed the increase in spatial resolution, which is ~5 times higher than confocal microscopy.

Thanks to the high spatial resolution of TEPL, spectral information that showcases heterogeneities could be extracted at the nanoscale. With diffraction-limited confocal microscopy, a slight spectral blue shift (shift of the peak position less than a few nm) of MoSe₂ luminescence in the vicinity of the heterojunction was seen (Figure 5a). However, thanks to the higher spatial resolution of the RE-TEPL, more complex heterogeneities could be revealed. As shown in Figure 5b, the position dependence of the blue shift was not as simple as found in confocal microscopy. First of all, the maximum shift found in this sample was ~5 nm. Second, the amount of shift at the hetero junction was not homogeneous along the heterojunction, where ~5 nm blue shift was found at the apex of the triangle shape of MoSe₂, while only ~2 nm shift was observed at the long side of the triangle. This blue shift was most likely due to local strain⁵² in the material and exciton migration.⁵¹ The spatial heterogeneity of the blue shift could reflect the heterogeneity of strain and/or exciton migration

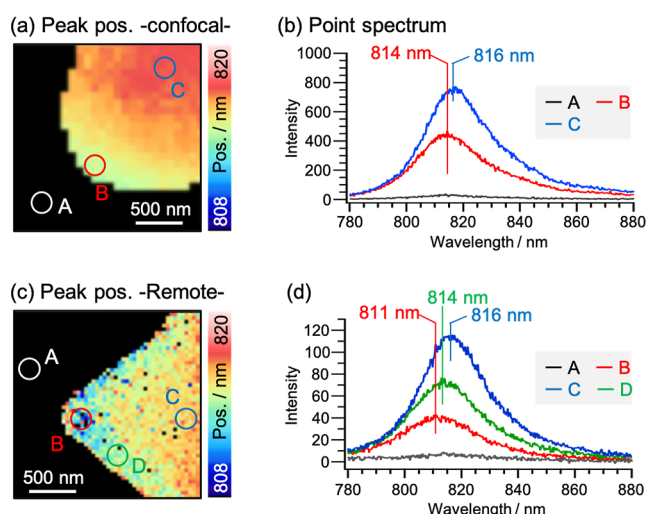


Figure 5. Mapping of the peak positions (left) and the recorded spectra of the circled areas (right) on a monolayer of the MoSe₂/WSe₂ lateral heterostructure on a Si/SiO₂ substrate, respectively, for (a,b) confocal microscopy, and (c,d) RE-TEPL.

dynamics. This high-resolution spectroscopic mapping thus truly showcases the ability of pNW coupler-mediated RE-TEPL to harvest further details of the local heterogeneity of nanomaterials. To further enhance the spatial resolution of RE-TEPL, two key factors can be explored: AgNW sharpness and the apex-to-sample distance. A sharper apex will decrease the excitation volume, while the optimized distance between the AgNW apex and the sample surface will lead to a higher PL enhancement, which could result in an improvement of spatial resolution.

CONCLUSIONS

This work demonstrates the increased coupling efficiency of a RE system consisting of two parallel AgNWs, compared to a more traditional system with *in situ*-grown Au nanoparticles on a AgNW. The results obtained showed that this system allows almost complete removal of the background signal generated by the far field, which led to a substantial increase in TEPL

contrast with a nongap mode configuration (or with a nonplasmonic substrate). The unprecedented performance of this work can greatly increase the image contrast and reveal heterogeneities of material properties that would be missed with any other known technique. Thus, the RE of TEF with the parallel nanowire coupler will open a new venue for luminescent material characterization at the nanoscale.

■ ASSOCIATED CONTENT

SI Supporting Information

The Supporting Information is available free of charge at <https://pubs.acs.org/doi/10.1021/acsomega.3c04952>.

Silver nanowire polyol synthesis and photoinduced growth of Au NPs on AgNW; parallel AgNW fabrication; schematic representation of setup used to manipulate AgNWs for parallel alignment and attachment to an AFM cantilever; schematic representation and transmission images of manipulation of AgNWs to form parallel AgNW, AgNWs drop-cast on the ITO substrate, pushing of AgNWs with an AFM cantilever to achieve alignment, picking up one AgNW, and redeposit the nanowire at the desired protrusion length and push them together; FDTD simulations; FDTD simulations to verify the reflection of the propagating SPPs by the coupling points; measurement of the far-field out-coupling light re-emitted from the apex end of the AgNW system; transmission images of RE probes, the red arrow indicates the RE coupling point, the cropped CCD image with the re-emitted light (color scales are not the same for both images); attaching the probe to the AFM cantilever; schematic representation and transmission image on how the AFM cantilever is positioned on the parallel AgNW probe to fabricate a RE-TES probe; laser misalignment estimation; simulation figures for different laser displacements, the laser is depicted in red, the sample in gray, RE-TES probe in black, and the pinhole inclusion volume in translucent white; MoSe₂/WSe₂ heterostructure; AFM topographic and phase images of a MoSe₂/WSe₂ heterostructure on a Si/SiO₂ substrate; Spectrum map around the junction; TEPL measurements; ray-path diagram of RE-TES setup; pinhole exclusion volume determination; and intensity plot of Rayleigh scattering in function of laser displacement (PDF)

■ AUTHOR INFORMATION

Corresponding Authors

Shuichi Toyouchi – *Division of Molecular Imaging and Photonics, Department of Chemistry, KU Leuven, Heverlee B-3001, Belgium*; Present Address: Research Institute for Light-Induced Acceleration System (RILACS), Osaka Metropolitan University, 1–2 Gakuen-cho, Naka-ku, Sakai, Osaka 599-8570, Japan; Email: shuichitoyouchi@omu.ac.jp

Yasuhiko Fujita – *Research Institute for Sustainable Chemistry, National Institute of Advanced Industrial Science and Technology (AIST Chugoku), Higashi-hiroshima, Hiroshima 739-0046, Japan*; orcid.org/0000-0003-1302-1436; Email: yasuhiko.fujita@aist.go.jp

Hiroshi Uji-i – *Division of Molecular Imaging and Photonics, Department of Chemistry, KU Leuven, Heverlee B-3001, Belgium; Institute for Integrated Cell-Material Science (WPI-*

iCeMS), Kyoto University, Kyoto 606-8501, Japan; RIES, Hokkaido University, Sapporo 001-0020, Japan; orcid.org/0000-0002-0463-9659; Email: hiroshi.ujii@kuleuven.be

Authors

Wannes Peeters – *Division of Molecular Imaging and Photonics, Department of Chemistry, KU Leuven, Heverlee B-3001, Belgium*

Mathias Wolf – *Division of Molecular Imaging and Photonics, Department of Chemistry, KU Leuven, Heverlee B-3001, Belgium*

Beatrice Fortuni – *Division of Molecular Imaging and Photonics, Department of Chemistry, KU Leuven, Heverlee B-3001, Belgium*; orcid.org/0000-0003-4634-9518

Eduard Fron – *Division of Molecular Imaging and Photonics, Department of Chemistry, KU Leuven, Heverlee B-3001, Belgium*; orcid.org/0000-0003-2260-0798

Tomoko Inose – *Institute for Integrated Cell-Material Science (WPI-iCeMS), Kyoto University, Kyoto 606-8501, Japan; The HAKUBI Center for Advanced Research, Kyoto University, Kyoto 606-8502, Japan*; orcid.org/0000-0003-2757-8817

Joan Hofkens – *Division of Molecular Imaging and Photonics, Department of Chemistry, KU Leuven, Heverlee B-3001, Belgium; Max Planck Institute for Polymer Research, Mainz 55128, Germany*; orcid.org/0000-0002-9101-0567

Takahiko Endo – *Department of Physics, Tokyo Metropolitan University, Hachioji, Tokyo 192-0397, Japan*; orcid.org/0000-0002-6520-6048

Yasumitsu Miyata – *Department of Physics, Tokyo Metropolitan University, Hachioji, Tokyo 192-0397, Japan*; orcid.org/0000-0002-9733-5119

Complete contact information is available at:

<https://pubs.acs.org/doi/10.1021/acsomega.3c04952>

Author Contributions

The manuscript was written through the contributions of all authors. All authors have given approval to the final version of the manuscript.

Notes

The authors declare no competing financial interest.

■ ACKNOWLEDGMENTS

This work was funded by the Research Foundation—Flanders. W.P. and B.F. acknowledge the support from FWO for the Ph.D. fellowships (1S53118N and 1S53120N) and the postdoctoral fellowships (12X1419N and 12X1423N), respectively. This work was also financially supported by the FWO research project (G081916N), the Japan Science and Technology Agency (JST), CREST (JPMJCR16F3) to Y.M., PRESTO (JPMJPR2104) to T.I., and the Japan Society for the Promotion of Science (JSPS) (JP18H01832, JP19KK0136, JP20K05413, JP21H04634, JP22K20512, JP22H00328, JP23H04877, JP23H01803, and JP23K17856). We also acknowledge the JSPS Core-to-Core Program, A., for the collaborative work.

■ ABBREVIATIONS

TEPL, tip-enhanced photoluminescence

TERS, tip-enhanced Raman spectroscopy

RE-TEPL, remote-excitation tip-enhanced photoluminescence
AuNP(s), gold nanoparticle(s)
AgNW(s), silver nanowire(s)
pNW, parallel nanowire
NP(s), nanoparticle(s)
DNA, deoxyribonucleic acid
STED, stimulated emission depletion
PALM, photoactivated localization microscopy
S-PALM, stroboscopic photoactivated localization microscopy
STORM, stochastic optical reconstruction microscopy
d-STORM, direct stochastic optical reconstruction microscopy
NASCA, nanometer accuracy by stochastic chemical reactions
TES, tip-enhanced spectroscopy
EM, electromagnetic
PL, photoluminescence
RE, remote excitation
SPPs, surface plasmon polaritons
LSPRs, localized surface plasmon resonances
CCD, charge-coupled device
SEM, scanning electron microscopy
ITO, indium tin oxide
SPM, scanning probe microscopy
AFM, atomic force microscopy
HOPG, highly ordered pyrolytic graphite
TMD, transition metal dichalcogenides

REFERENCES

- (1) Wang, Q. H.; Kalantar-Zadeh, K.; Kis, A.; Coleman, J. N.; Strano, M. S. Electronics and optoelectronics of two-dimensional transition metal dichalcogenides. *Nat. Nanotechnol.* **2012**, *7* (11), 699–712.
- (2) Lee, H.; Ahn, J.; Im, S.; Kim, J.; Choi, W. High-Responsivity Multilayer MoSe₂ Phototransistors with Fast Response Time. *Sci. Rep.* **2018**, *8* (1), 11545.
- (3) Ross, J. S.; Rivera, P.; Schaibley, J.; Lee-Wong, E.; Yu, H.; Taniguchi, T.; Watanabe, K.; Yan, J.; Mandrus, D.; Cobden, D.; Yao, W.; Xu, X. Interlayer Exciton Optoelectronics in a 2D Heterostructure p-n Junction. *Nano Lett.* **2017**, *17* (2), 638–643.
- (4) Liu, D.-N.; Guo, Y. Optoelectronic superlattices based on 2D transition metal dichalcogenides. *Appl. Phys. Lett.* **2021**, *118* (12), 123101.
- (5) Ma, Z.; Gerton, J. M.; Wade, L. A.; Quake, S. R. Fluorescence Near-Field Microscopy of DNA at Sub-10 nm Resolution. *Phys. Rev. Lett.* **2006**, *97* (26), 260801–260804.
- (6) Neely, R. K.; Deen, J.; Hofkens, J. Optical mapping of DNA: Single-molecule-based methods for mapping genomes. *Biopolymers* **2011**, *95* (5), 298–311.
- (7) Lipiec, E.; Sekine, R.; Bielecki, J.; Kwiatek, W. M.; Wood, B. R. Molecular Characterization of DNA Double Strand Breaks with Tip-Enhanced Raman Scattering. *Angew. Chem.* **2014**, *126* (1), 173–176.
- (8) He, Z.; Han, Z.; Kizer, M.; Linhardt, R. J.; Wang, X.; Sinyukov, A. M.; Wang, J.; Deckert, V.; Sokolov, A. V.; Hu, J.; Scully, M. O. Tip-Enhanced Raman Imaging of Single-Stranded DNA with Single Base Resolution. *J. Am. Chem. Soc.* **2019**, *141* (2), 753–757.
- (9) Wood, B. R.; Asghari-Khiavi, M.; Bailo, E.; McNaughton, D.; Deckert, V. Detection of Nano-Oxidation Sites on the Surface of Hemoglobin Crystals Using Tip-Enhanced Raman Scattering. *Nano Lett.* **2012**, *12* (3), 1555–1560.
- (10) Xiao, L.; Wang, H.; Schultz, Z. D. Selective Detection of RGD-Integrin Binding in Cancer Cells Using Tip Enhanced Raman Scattering Microscopy. *Anal. Chem.* **2016**, *88* (12), 6547–6553.
- (11) Rayleigh, L. XXXI Investigation in Optics, with special reference to the Spectroscope. *London, Edinburgh Dublin Philos. Mag. J. Sci.* **1879**, *8* (49), 261–274.
- (12) Klar, T. A.; Hell, S. W. Subdiffraction resolution in far-field fluorescence microscopy. *Opt. Lett.* **1999**, *24* (14), 954–956.
- (13) Bancelin, S.; Mercier, L.; Murana, E.; Nägerl, U. V. Aberration correction in stimulated emission depletion microscopy to increase imaging depth in living brain tissue. *Neurophotonics* **2021**, *8* (03), 035001.
- (14) Bodén, A.; Pennacchietti, F.; Coceano, G.; Damenti, M.; Ratz, M.; Testa, I. Volumetric live cell imaging with three-dimensional parallelized RESOLFT microscopy. *Nat. Biotechnol.* **2021**, *39* (5), 609–618.
- (15) Betzig, E.; Patterson, G. H.; Sougrat, R.; Lindwasser, O. W.; Olenych, S.; Bonifacino, J. S.; Davidson, M. W.; Lippincott-Schwartz, J.; Hess, H. F. Imaging Intracellular Fluorescent Proteins at Nanometer Resolution. *Science* **2006**, *313* (5793), 1642–1645.
- (16) Flors, C.; Hotta, J.-I.; Uji-i, H.; Dedecker, P.; Ando, R.; Mizuno, H.; Miyawaki, A.; Hofkens, J. A Stroboscopic Approach for Fast Photoactivation-Localization Microscopy with Dronpa Mutants. *J. Am. Chem. Soc.* **2007**, *129* (45), 13970–13977.
- (17) Nehme, E.; Weiss, L. E.; Michaeli, T.; Shechtman, Y. Deep-STORM: Super-resolution single-molecule microscopy by deep learning. *Optica* **2018**, *5* (4), 458–464.
- (18) Rust, M. J.; Bates, M.; Zhuang, X. Sub-diffraction-limit imaging by stochastic optical reconstruction microscopy (STORM). *Nat. Methods* **2006**, *3* (10), 793–796.
- (19) Van De Linde, S.; Löschberger, A.; Klein, T.; Heidbreder, M.; Wolter, S.; Heilemann, M.; Sauer, M. Direct stochastic optical reconstruction microscopy with standard fluorescent probes. *Nat. Protoc.* **2011**, *6* (7), 991–1009.
- (20) Roeloffs, M. B. J.; De Cremer, G.; Libeert, J.; Ameloot, R.; Dedecker, P.; Bons, A.-J.; Bückins, M.; Martens, J. A.; Sels, B. F.; De Vos, D. E.; Hofkens, J. Super-Resolution Reactivity Mapping of Nanostructured Catalyst Particles. *Angew. Chem., Int. Ed.* **2009**, *48* (49), 9285–9289.
- (21) Sonntag, M. D.; Pozzi, E. A.; Jiang, N.; Hersam, M. C.; Van Duyne, R. P. Recent Advances in Tip-Enhanced Raman Spectroscopy. *J. Phys. Chem. Lett.* **2014**, *5* (18), 3125–3130.
- (22) Zhang, K.; Bao, Y.; Cao, M.; Taniguchi, S.-i.; Watanabe, M.; Kambayashi, T.; Okamoto, T.; Haraguchi, M.; Wang, X.; Kobayashi, K.; Yamada, H.; Ren, B.; Tachizaki, T. Low-Background Tip-Enhanced Raman Spectroscopy Enabled by a Plasmon Thin-Film Waveguide Probe. *Anal. Chem.* **2021**, *93* (21), 7699–7706.
- (23) Walke, P.; Fujita, Y.; Peeters, W.; Toyouchi, S.; Fredericks, W.; De Feyter, S.; Uji-i, H. Silver nanowires for highly reproducible cantilever based AFM-TERS microscopy: towards a universal TERS probe. *Nanoscale* **2018**, *10* (16), 7556–7565.
- (24) Fujita, Y.; Walke, P.; De Feyter, S.; Uji-i, H. Tip-enhanced Raman scattering microscopy: Recent advance in tip production. *Jpn. J. Appl. Phys.* **2016**, *55* (8S1), 08NA02.
- (25) Fujita, Y.; Walke, P.; Feyter, S. D.; Uji-i, H. Remote excitation-tip-enhanced Raman scattering microscopy using silver nanowire. *Jpn. J. Appl. Phys.* **2016**, *55* (8S1), 08NB03.
- (26) Wang, C.-F.; Zamkov, M.; El-Khoury, P. Z. Ambient Tip-Enhanced Photoluminescence with 5 nm Spatial Resolution. *J. Phys. Chem. C* **2021**, *125* (22), 12251–12255.
- (27) Lee, H.; Lee, D. Y.; Kang, M. G.; Koo, Y.; Kim, T.; Park, K.-D. Tip-enhanced photoluminescence nano-spectroscopy and nano-imaging. *Nanophotonics* **2020**, *9* (10), 3089–3110.
- (28) Jiang, N.; Kurouski, D.; Pozzi, E. A.; Chiang, N.; Hersam, M. C.; Van Duyne, R. P. Tip-enhanced Raman spectroscopy: From concepts to practical applications. *Chem. Phys. Lett.* **2016**, *659*, 16–24.
- (29) Martin, O. J. F.; Girard, C. Controlling and tuning strong optical field gradients at a local probe microscope tip apex. *Appl. Phys. Lett.* **1997**, *70* (6), 705–707.
- (30) Liao, P. F.; Wokaun, A. Lightning rod effect in surface enhanced Raman scattering. *J. Chem. Phys.* **1982**, *76* (1), 751–752.

- (31) Willets, K. A.; Van Duyne, R. P. Localized surface plasmon resonance spectroscopy and sensing. *Annu. Rev. Phys. Chem.* **2007**, *58* (1), 267–297.
- (32) Wu, Z.-Q.; Yang, J.-L.; Manjunath, N. K.; Zhang, Y.-J.; Feng, S.-R.; Lu, Y.-H.; Wu, J.-H.; Zhao, W.-W.; Qiu, C.-Y.; Li, J. F.; Lin, S.-S. Gap-Mode Surface-Plasmon-Enhanced Photoluminescence and Photoresponse of MoS₂. *Adv. Mater.* **2018**, *30* (27), No. e1706527.
- (33) Nordlander, P.; Prodan, E. Plasmon Hybridization in Nanoparticles near Metallic Surfaces. *Nano Lett.* **2004**, *4* (11), 2209–2213.
- (34) Park, K.-D.; Jiang, T.; Clark, G.; Xu, X.; Raschke, M. B. Radiative control of dark excitons at room temperature by nano-optical antenna-tip Purcell effect. *Nat. Nanotechnol.* **2018**, *13* (1), 59–64.
- (35) Carminati, R.; Greffet, J. J.; Henkel, C.; Vigoureux, J. M. Radiative and non-radiative decay of a single molecule close to a metallic nanoparticle. *Opt. Commun.* **2006**, *261* (2), 368–375.
- (36) Yang, B.; Chen, G.; Ghafoor, A.; Zhang, Y.; Zhang, Y.; Zhang, Y.; Luo, Y.; Yang, J.; Sandoghdar, V.; Aizpurua, J.; Dong, Z.; Hou, J. G. Sub-nanometre resolution in single-molecule photoluminescence imaging. *Nat. Photonics* **2020**, *14* (11), 693–699.
- (37) Su, L.; Lu, G.; Kenens, B.; Rocha, S.; Fron, E.; Yuan, H.; Chen, C.; Van Dorpe, P.; Roeffaers, M. B. J.; Mizuno, H.; Hofkens, J.; Hutchison, J. A.; Uji-i, H. Visualization of molecular fluorescence point spread functions via remote excitation switching fluorescence microscopy. *Nat. Commun.* **2015**, *6*, 6287.
- (38) Hutchison, J. A.; Centeno, S. P.; Odaka, H.; Fukumura, H.; Hofkens, J.; Uji-i, H. Subdiffraction Limited, Remote Excitation of Surface Enhanced Raman Scattering. *Nano Lett.* **2009**, *9* (3), 995–1001.
- (39) de Torres, J.; Ferrand, P.; Colas des Francs, G.; Wenger, J. Coupling Emitters and Silver Nanowires to Achieve Long-Range Plasmon-Mediated Fluorescence Energy Transfer. *ACS Nano* **2016**, *10* (4), 3968–3976.
- (40) Ma, X.; Zhu, Y.; Yu, N.; Kim, S.; Liu, Q.; Apontti, L.; Xu, D.; Yan, R.; Liu, M. Toward High-Contrast Atomic Force Microscopy-Tip-Enhanced Raman Spectroscopy Imaging: Nanoantenna-Mediated Remote-Excitation on Sharp-Tip Silver Nanowire Probes. *Nano Lett.* **2019**, *19* (1), 100–107.
- (41) Johnson, P. B.; Christy, R. W. Optical Constants of the Noble Metals. *Phys. Rev. B: Solid State* **1972**, *6* (12), 4370–4379.
- (42) Kretschmann, E.; Raether, H. Radiative Decay of Non Radiative SURface Plasmons Excited by Light. *Z. Naturforsch., A: Astrophys., Phys. Phys. Chem.* **1968**, *23*, 2135–2136.
- (43) Knight, M. W.; Grady, N. K.; Bardhan, R.; Hao, F.; Nordlander, P.; Halas, N. J. Nanoparticle-Mediated Coupling of Light into a Nanowire. *Nano Lett.* **2007**, *7* (8), 2346–2350.
- (44) Sanders, A. W.; Routenberg, D. A.; Wiley, B. J.; Xia, Y.; Dufresne, E. R.; Reed, M. A. Observation of Plasmon Propagation, Redirection, and Fan-Out in Silver Nanowires. *Nano Lett.* **2006**, *6* (8), 1822–1826.
- (45) Berweger, S.; Atkin, J. M.; Olmon, R. L.; Raschke, M. B. Adiabatic Tip-Plasmon Focusing for Nano-Raman Spectroscopy. *J. Phys. Chem. Lett.* **2010**, *1* (24), 3427–3432.
- (46) Umakoshi, T.; Saito, Y.; Verma, P. Highly efficient plasmonic tip design for plasmon nanofocusing in near-field optical microscopy. *Nanoscale* **2016**, *8* (10), 5634–5640.
- (47) Toyouchi, S.; Wolf, M.; Nakao, Y.; Fujita, Y.; Inose, T.; Fortuni, B.; Hirai, K.; Hofkens, J.; De Feyter, S.; Hutchison, J.; Uji-i, H. Controlled Fabrication of Optical Signal Input/Output Sites on Plasmonic Nanowires. *Nano Lett.* **2020**, *20* (4), 2460–2467.
- (48) Inose, T.; Toyouchi, S.; Lu, G.; Umemoto, K.; Tezuka, Y.; Lyu, B.; Masuhara, A.; Fron, E.; Fujita, Y.; Hirai, K.; Uji-i, H. Water-mediated polyol synthesis of pencil-like sharp silver nanowires suitable for nonlinear plasmonics. *Chem. Commun.* **2019**, *55* (77), 11630–11633.
- (49) Khurgin, J. B. How to deal with the loss in plasmonics and metamaterials. *Nat. Nanotechnol.* **2015**, *10* (1), 2–6.
- (50) Wada, N.; Pu, J.; Takaguchi, Y.; Zhang, W.; Liu, Z.; Endo, T.; Irisawa, T.; Matsuda, K.; Miyauchi, Y.; Takenobu, T.; Miyata, Y. Efficient and Chiral Electroluminescence from In Plane Heterostructure of Transition Metal Dichalcogenide Monolayers. *Adv. Funct. Mater.* **2022**, *32* (40), 2203602.
- (51) Shimasaki, M.; Nishihara, T.; Matsuda, K.; Endo, T.; Takaguchi, Y.; Liu, Z.; Miyata, Y.; Miyauchi, Y. Directional Exciton-Energy Transport in a Lateral Heteromonolayer of WSe₂-MoSe₂. *ACS Nano* **2022**, *16* (5), 8205–8212.
- (52) Park, K.-D.; Khatib, O.; Kravtsov, V.; Clark, G.; Xu, X.; Raschke, M. B. Hybrid Tip-Enhanced Nanospectroscopy and Nanoimaging of Monolayer WSe₂ with Local Strain Control. *Nano Lett.* **2016**, *16* (4), 2621–2627.